FINAL REPORT

INVESTIGATION OF A REAL-TIME PROCESSING SYSTEM FOR THE NASA MULTIFREQUENCY MICROWAVE RADIOMETER

CONTRACT NAS 9-14821

June 11, 1976

TEXAS A&M UNIVERSITY
REMOTE SENSING CENTER
COLLEGE STATION, TEXAS

FINAL REPORT

INVESTIGATION OF A REAL-TIME PROCESSING SYSTEM FOR THE NASA MULTIFREQUENCY MICROWAVE RADIOMETER

Contract NAS 9-14821

June 11, 1976

Final Report RSC 3313-1

INVESTIGATION OF A REAL-TIME PROCESSING SYSTEM FOR THE NASA MULTIFREQUENCY MICROWAVE RADIOMETER

Contract NAS 9-14821

June 11, 1976

INTRODUCTION

The Remote Sensing Center at Texas A&M University (TAMU) has conducted a study for the National Aeronautics and Space Administration, L. B. Johnson Space Center (NASA/JSC) investigating the data reduction and processing requirements for the NASA/JSC Multifrequency Microwave Radiometer (MFMR) system. The objectives of the investigation were to develop and evaluate algorithms and processing techniques which might provide for dedicated real-time or near real-time data processing and to develop a configuration design and processor recommendation to accomplish the data reduction.

The scope of the study included an analysis of the required data reduction and calibration equations, the identification of sources of error which may be present in the MFMR data, and the definition and evaluation

of the significance of effects introduced by aircraft perturbation.

The specific tasks defining the steps necessary for achieving the objectives of the research and development effort were identified as the following:

A. Definition of System Errors

B. Definition of Aircraft Perturbation Effects

C. Definition of Special Signal Processing Needs

D. Evaluation of Current Processing Techniques and Approaches

E. Definition of Signal Processing Plan

F. System Design of Processor

The documentation of the results of these tasks begins with a general description of the MFMR system and identifies the key components of the data calibration and correction algorithm. The evaluation of current processing techniques and approaches (Task D) follows a careful analysis of the MFMR system errors (Task A) which includes errors due to radome, antenna and waveguide effects and aircraft perturbation effects (Task B). Based on these analyses, it is concluded that the present data calibration and correction algorithms are adequate for providing the kinds of data products desired for MFMR applications.

It is further concluded, based upon a careful study of the MFMR system output signals and corresponding timing requirements (Task C), that real-time processing of MFMR data is indeed feasible by utilizing processing techniques similar to those developed by TAMU for the NASA/JSC 13.3 GHz Scatterometer. A signal processing plan (Task E) and a system design (Task F) are presented which specify a real-time processing system for the NASA Multifrequency Microwave Radiometer.

THE MFMR SYSTEM

The MFMR System consists of a cluster of four distinct microwave radiometers, each with its own antenna, reference noise generators, RF and IF circuitry, and analog data outputs. Each radiometer is identified by a frequency band designated according to the center frequency of operation. The band designations and corresponding center frequencies are:

L-band - 1.4135 GHz

K_u-band - 18.0 GHz

K-band - 22.05 GHZ

K_a-band - 37.0 GHz

The K_u-, K-, and K_a-band units are dual polarization radiometers, while the L-band unit receives only a

single linear polarization. The L-band polarization orientation (i.e., vertical or horizontal) may be selected by means of mechanical rotation of the antenna mount. Rotation of the antenna mount rotates all four radiometer receivers and antennas, and consequently, the polarization designations for the dual polarized radiometers are reversed. The antennas and receiver enclosures are mounted under the nose radome of the NASA/JSC P3-A aircraft. The antenna elevation angle (and consequently, the nominal angle of incidence) is also controlled by mechanical positioning of the antenna. The antenna elevation angle is selectable from zero (nadir) to 180 degrees (zenith) and is maintained at a fixed angle with respect to the airplane during an operational data collection run. The Antenna Position Control/Master Control Panel, located at the MFMR operator's station within the aircraft, provides for direct control of all aspects of in-flight system operation.

The seven analog output signals of the radiometer receivers, the temperature monitoring thermister signals, and the AGC voltage signals are digitized and multiplexed along with receiver mode and antenna position codes into a single channel PCM digital data stream for recording on one channel of a 14-track, 1 inch Micom Series 110 Recorder.

Each radiometer receiver is configured as an AGC stablized Dicke Radiometer which employs two stable reference loads (noise sources) and synchronous demodulation techniques to yield a very sensitive measurement of the power incident upon the receiver antenna, expressed in terms of an apparent brightness temperature.

A thorough discussion of the design of the MFMR L-band receiver, which is also applicable to the other receivers, is given by Reid [1].

The necessary equations for computing the receiver input radiometric temperature (which may alsc be termed the uncorrected brightness temperature) from the measured output voltage are also documented by Reid [2]. The receiver input temperature is said to be uncorrected because the calibration equation references the measured received power to the input port of the receiver only. Additional corrections must be applied to account for waveguide, antenna and radome losses. All of these corrections depend upon measuring the thermometric temperature of these components and, for the case of the antennas and radome, are a function of antenna position.

The calibration and data reduction equations are repeated here without development. The uncorrected

radiometric brightness temperature T_B' is computed from a linear calibration equation as

$$T_B' = T_1 + \Delta T \left[\frac{\overline{C}_A - \overline{C}_B}{\overline{C}_C - \overline{C}_B} \right] \quad (1)$$

where

T_1 = calibration line intercept

ΔT = calibration line slope

$\overline{C}_A$ = average radiometer output data count in the operate mode

$\overline{C}_B$ = average radiometer output data count in the base-line mode

$\overline{C}_C$ = average radiometer output data count in the calibrate mode.

T_1 and ΔT are determined from laboratory calibration procedures in which known hot and cold reference loads are connected to the radiometer input port and the corresponding output is measured. Equation (1) may be rearranged slightly to simplify its appearance as follows.

$$T_B' = \left\{ T_1 - \frac{\Delta T \, \overline{C}_B}{[\overline{C}_C - \overline{C}_B]} \right\} + \left\{ \frac{\Delta T}{[\overline{C}_C - \overline{C}_B]} \right\} \overline{C}_A \quad (2)$$

or

$$T_B' = T_{BL} + SF \cdot \overline{C}_A \quad (3)$$

where

T_{BL} = baseline temperature, computed from the first two terms of (2)

SF = scale factor = $\Delta T / [\overline{C}_C - \overline{C}_B]$

For either equation (1) or equation (3) it is observed that prior to calculating T_B' in the operate mode, values of $\overline{C}_C$ and $\overline{C}_B$ must be determined by operating the system in the calibrate and baseline modes, respectively.

Once the calibration constants have been determined and a value of T_B' has been computed, the correction equations for referencing the observed input temperature to the true physical input port of the system (i.e., the nose radome of the P3-A) can be applied

$$T_B = L_R L_A L_W (T_B' - T_W) + L_R L_A (T_W - T_A) + L_R (T_A - T_R) + T_R \quad (4)$$

where

T_B = corrected input brightness temperature

T_R = physical temperature of the radome

T_A = physical temperature of the antenna

T_W = physical temperature of the waveguide (or cable) connecting the antenna to the radiometer input port

L_R = radome loss factor (in general a function of frequency, antenna position and polarization)

L_A = antenna loss factor (one value for each frequency and polarization)

L_W = waveguide (or cable) loss factor

The physical temperatures in equation (4) are measured by means of thermistors mounted on the respective components. The thermistor resistance measurements, expressed in terms of PCM counts in the output data stream, are converted to temperatures by means of a polynomial of order five to seven depending upon the particular thermistor involved.

The loss factors are independently measured quantities which are assumed to be constant. The radome loss factors are provided for each frequency and polarization at elevation angles from 0 to 180 degrees in five degree increments.

The end product of the data reduction and correction processing consists of corrected apparent brightness temperatures for each of seven radiometer output channels, identified by frequency, polarization and angle of incidence, averaged over a specified time interval dependent upon the required resolution cell size and

temperature sensitivity. In addition, the standard deviation of the data samples that are averaged to produce a single data point is computed for each channel. The resulting data frame is identified by a time code to provide a means for correlating the MFMR to other sensor data (e.g., photographic imagery) and ultimately to a known target cell along the flight line.

MFMR SYSTEM ERRORS

As with any measuring or sensing device, errors exist in the MFMR output for which correction by appropriate data processing algorithms is desirable. Correction for errors due to the radome, antenna and waveguide effects are expressed in terms of the loss factors in equation (4). The extent to which these factors accurately account for these effects is limited by the precision to which the loss factors and component temperatures can be measured and by the magnitude of the reflection coefficients due to mismatch at the component interfaces. Component mismatch error can be included in the loss factor terms but these "effective" loss factors are functions of component temperature.

Extreme operating environmental temperatures can also invalidate the loss factor corrections, particularly at low temperatures. Contact with Mr. Al Chang at NASA/Goddard

Space Flight Center, who has had occasion to analyze MFMR data for flights in the Arctic regions, reveals that use of the standard loss factor corrections for such data results in very large errors in the computed brightness temperatures. These temperature effects can most probably be attributed to condensed water or ice on the antennas or inside the input waveguides.

While noting that temperature dependent errors may exist in the MFMR data that are not corrected by present processing techniques, it does not appear feasible to attempt the extensive measurements necessary in order to obtain correction factors as a function of environmental temperature. A more resonable approach would be to define a nominal operating range, representative of the majority of MFMR missions for which the present correction equations are known to be quite adequate. For those missions which involve extreme temperature ranges, a secondary calibration method - that of correcting the data based upon measurement over some known target - could be employed.

In addition to the errors introduced by system losses and component mismatch, there are secondary effects present in the MFMR data which are caused by aircraft perturbations off the ideal case of straight, level flight. These affects are termed "secondary" because unlike the

NASA scatterometer systems whose geometric, resolution and calibration parameters depend explicitly on aircraft state, the MFMR calibration does not depend directly on the orientation and velocity of the aircraft platform. For the MFMR, deviations in the aircraft state from straight level flight introduces a displacement in the location of the target cell, alters the effective angle of incidence and introduces an effective polarization rotation.

Consider first the displacement of the target cell location off the true flight line. For purposes of analysis, select a coordinate system which has its origin centered at the aircraft center of mass (which, with insignificant error, is also assumed to be the MFMR antenna location). Assume the principle coordinate axes are defined such that the x-axis extends to the right of the aircraft in the cross-track direction. As shown in Figure 1, the center of the instantaneous target cell is located at the intersection of a line through the antenna boresight axis with the ground, defined by a plane at $z = -h$. The equation for the antenna axis center line under zero perturbation conditions is,

$$\frac{x}{\cos \pi/2} = \frac{y}{\sin \theta} = \frac{-z}{\cos \theta} \qquad (5)$$

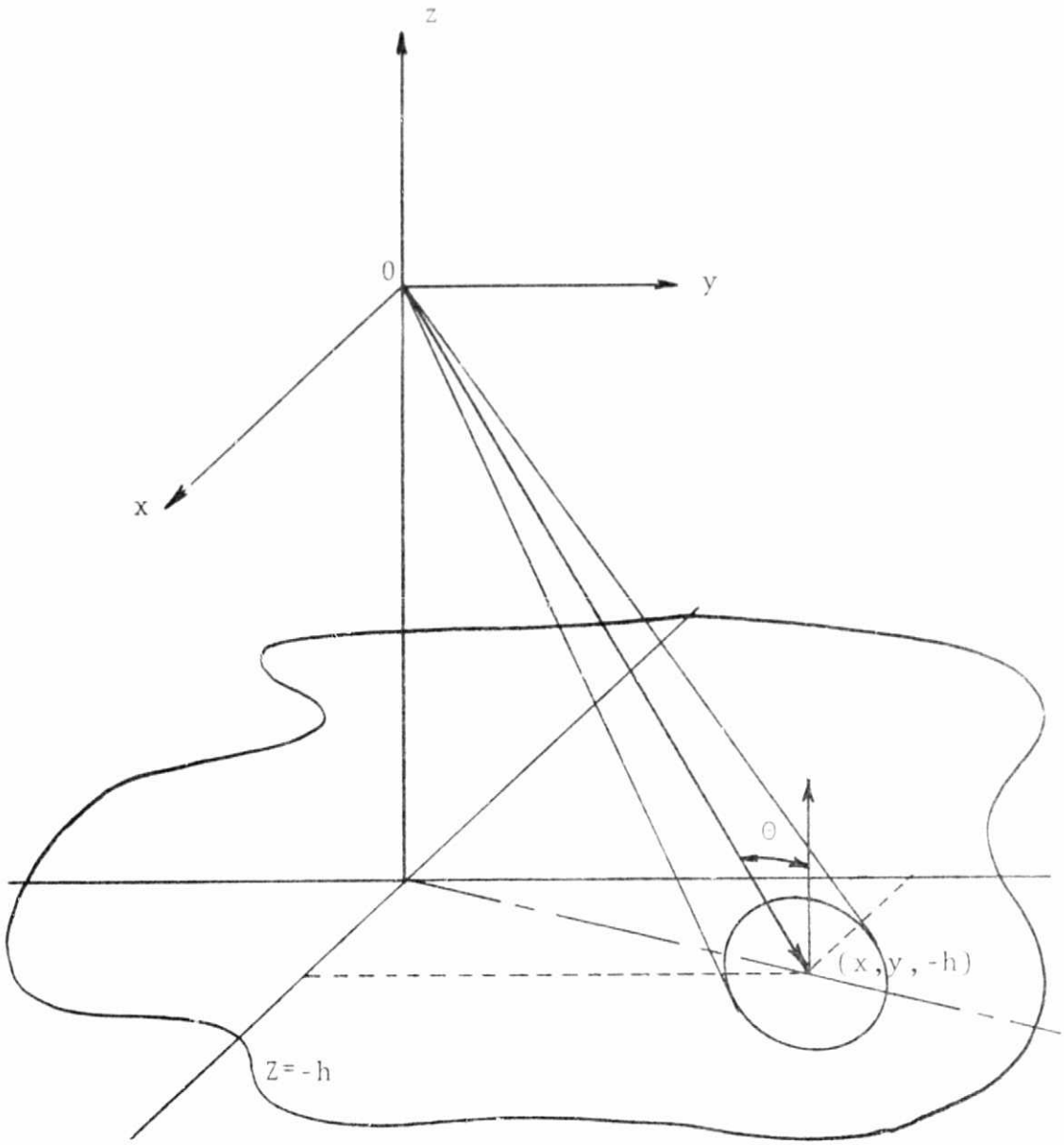

Figure 1. MFMR Geometry

where θ is the look angle of the antenna with respect to aircraft nadir. Introducing aircraft roll (ε), pitch (α) and drift (Ψ) modifies (5) as,

$$\frac{-x}{\cos\varepsilon \sin\psi \sin\theta + \sin\varepsilon \cos\theta} \tag{6}$$

$$= \frac{y}{\sin\theta(\cos\alpha\cos\psi - \sin\alpha\sin\varepsilon\sin\psi) + \sin\alpha\cos\varepsilon\cos\theta}$$

$$= \frac{z}{(\cos\alpha\sin\varepsilon\sin\psi + \sin\alpha\cos\psi)\sin\theta - \cos\alpha\cos\varepsilon\cos\theta}$$

From (6), both the x and y coordinates of the target cell center are easily obtained by setting z = -h and evaluating the various sines and cosines for given aircraft state and antenna position angles.

By comparing (5) and (6) and recalling that the true angle of incidence is defined to be the angle between the surface normal (in this case, the z-axis) and the antenna axis center-line (i.e., the direction of the propagation vector of the electromagnetic radiation), it is observed that the effective angle of incidence is given by

$$\theta_{eff} = \cos^{-1}\Big[-(\cos\alpha\sin\varepsilon\sin\psi + \alpha\cos\psi)\sin\theta + \cos\alpha\cos\varepsilon\cos\theta\Big] \tag{7}$$

To indicate the general behavior of each perturbation effect, equation (7) may be simplified by considering one non-zero parameter at a time as follows:

Roll only: $$\theta_{eff} = \cos^{-1}(\cos\epsilon\cos\theta) \tag{8a}$$

Drift only; $$\theta_{eff} = \theta \tag{8b}$$

Pitch only; $$\theta_{eff} = \theta + \alpha \tag{8c}$$

An additional effect of aircraft perturbation, in particular, aircraft roll, is to rotate the polarization axes of the antennas with respect to the vertical and horizontal polarization axes defined with respect to the direction of propagation and the surface normal. The amount of depolarization which occurs (at the beam center) is a function of the effective angle of incidence, with the greatest effect occurring at nadir.

To determine the depolarization effects analytically, consider polarization axes of the antennas written in terms of unit vectors defined as follows,

$$\hat{\ell}_v = \cos\theta\,\hat{a}_y + \sin\theta\,\hat{a}_z \tag{9a}$$

$$\hat{\ell}_h = \hat{a}_x \tag{9b}$$

where

$\hat{\ell}_v$ = vertical polarization vector

$\hat{\ell}_h$ = horizontal polarization vector

Θ = antenna position angle

The corresponding surface polarization vectors may be found by first taking the vector cross product of the propagation unit vector $\hat{k}$ with the surface normal $\hat{n}$ and normalizing to obtain the horizontal vector $\hat{h}$. Taking a second cross product, between $\hat{h}$ and $\hat{k}$, gives the vertical vector $\hat{v}$.

The propagation vector $\hat{k}_o$ under zero roll conditions may be written as

$$\begin{aligned}\hat{k}_o &= \cos\tfrac{\pi}{2}\,\hat{a}_x + \cos(\tfrac{\pi}{2}-\theta)\,\hat{a}_y + \cos(\pi-\theta)\,\hat{a}_z \\ &= 0\cdot\hat{a}_x + \sin\theta\,\hat{a}_y - \cos\theta\,\hat{a}_z\end{aligned} \tag{10}$$

The surface normal written in terms of coordinate unit vectors is simply

$$\hat{n} = \hat{a}_z \tag{11}$$

Thus, $\hat{h}_o$ may be found as

$$\begin{aligned}\hat{h}_o &= \frac{\hat{k}_o \times \hat{n}}{|\hat{k}_o \times \hat{n}|} \\ &= \frac{\sin\theta\,(\hat{a}_y \times \hat{a}_z) - \cos\theta\,(a_z \times a_z)}{|\sin\theta|} \\ &= \hat{a}\end{aligned} \tag{12}$$

Similarly, $\hat{v}_o$ is found as

$$\begin{aligned} \hat{v}_o &= \hat{h}_o \times \hat{k}_o \\ &= a_x \times (\sin\theta\, \hat{a}_y - \cos\theta\, \hat{a}_z) \\ &= \cos\theta\, \hat{a}_y + \sin\theta\, \hat{a}_z \end{aligned} \tag{13}$$

To obtain the response of the antenna to the defined surface polarizations it is only necessary to take the dot product of the polarization vectors and antenna axis vectors.

$$\begin{aligned} V_l &= \hat{l}_v \cdot \hat{v}_o \\ &= (\cos\theta\, \hat{a}_y + \sin\theta\, \hat{a}_z) \cdot (\cos\theta\, \hat{a}_y + \sin\theta a_z) \\ &= \cos^2\theta + \sin^2\theta = 1 \end{aligned} \tag{14a}$$

$$\begin{aligned} V_c &= \hat{l}_v \cdot \hat{h}_o \\ &= (\cos\theta\, \hat{a}_y + \sin\theta\, \hat{a}_z) \cdot \hat{a}_x \\ &= 0 \end{aligned} \tag{14b}$$

$$\begin{aligned} H_l &= \hat{l}_h \cdot \hat{h}_o \\ &= \hat{a}_x \cdot \hat{a}_x \\ &= 1 \end{aligned} \tag{14c}$$

$$\begin{aligned} H_c &= \hat{l}_h \cdot \hat{v}_o \\ &= \hat{a}_x \cdot (\cos\theta\, \hat{a}_y + \sin\theta\, \hat{a}_z) \\ &= 0 \end{aligned} \tag{14d}$$

where

V_ℓ = antenna vertical polarization like response

V_c = antenna vertical polarization cross response

H_ℓ = antenna horizontal polarization like response

H_c = antenna horizontal polarization cross response

As is evident from equations (14a-d), for zero roll conditions, the surface and antenna polarizations (at the beam center) coincide and provide the desired polarization measurements.

Now consider the effects of aircraft roll. The antenna polarization axes become

$$\hat{\ell}_v = -\sin\varepsilon \sin\theta \hat{a}_x + \cos\theta \hat{a}_y + \cos\varepsilon \sin\theta \hat{a}_z \quad (15a)$$

$$\hat{\ell}_h = \cos\varepsilon \hat{a}_x + \sin\varepsilon \hat{a}_z \quad (15b)$$

The propagation unit vector becomes

$$\hat{k} = \sin\varepsilon\cos\theta\,\hat{a}_x + \sin\theta\,\hat{a}_y - \cos\varepsilon\cos\theta\,\hat{a}_z \qquad (16)$$

The surface polarization vectors are again found by the previously specified cross products as

$$\hat{h} = \frac{\hat{k}\times\hat{n}}{|\hat{k}\times\hat{n}|} \qquad (17a)$$

$$= \frac{\sin\varepsilon\cos\theta\,(\hat{a}_x\times\hat{a}_z) + \sin\theta\,(\hat{a}_y\times\hat{a}_z)}{(\sin^2\varepsilon\cos^2\theta + \sin^2\theta)^{\frac{1}{2}}}$$

$$= \frac{\sin\theta\,\hat{a}_x - \sin\varepsilon\cos\theta\,\hat{a}_y}{(\sin^2\varepsilon\cos^2\theta + \sin^2\theta)^{\frac{1}{2}}}$$

$$\hat{v} = \hat{h}\times\hat{k} \qquad (17b)$$

$$= \frac{\cos^2\theta\cos\varepsilon\sin\varepsilon\,\hat{a}_x + \cos\varepsilon\sin\theta\cos\theta\,\hat{a}_y + (\sin^2\theta + \sin^2\varepsilon\cos^2\theta)\hat{a}_z}{(\sin^2\varepsilon\cos^2\theta + \sin^2\theta)^{\frac{1}{2}}}$$

Again the antenna response is computed as in (14a-d)

$$V_l = \frac{\cos\varepsilon \sin\theta}{(\sin^2\varepsilon \cos^2\theta + \sin^2\theta)^{\frac{1}{2}}} \tag{18a}$$

$$V_c = \frac{-\sin\varepsilon}{(\sin^2\varepsilon \cos^2\theta + \sin^2\theta)^{\frac{1}{2}}} \tag{18b}$$

$$H_l = \frac{\cos\varepsilon \sin\theta}{(\sin^2\varepsilon \cos^2\theta + \sin^2\theta)^{\frac{1}{2}}} \tag{18c}$$

$$H_c = \frac{\sin\varepsilon}{(\sin^2\varepsilon \cos^2\theta + \sin^2\theta)^{\frac{1}{2}}} \tag{18d}$$

The expressions (18a-d) described the response to the electric fields incident upon the antenna due to vertically and horizontally polarized energy emitted from the target surface in the direction of the receiving antenna. To describe the relative response in terms of power, and consequently in terms of apparent temperature, requires the coefficients V_1, V_c, H_1 , and H_c be squared. The measured response is then written as

$$T_{vm} = V_\ell^2 T_v + V_c^2 T_h \qquad (19a)$$

$$T_{hm} = H_c^2 T_v + H_\ell^2 T_h \qquad (19b)$$

where

T_{vm} = measured vertical apparent temperature

T_{hm} = measured horizontal apparent temperature

T_v = true vertical apparent temperature

T_h = true horizontal apparent temperature

For the case of the K_u-, K-, and K_a-band systems, both T_{vm} and T_{hm} are obtained simultaneously, which allows for inversion of equations (19a-b). That is

$$\begin{bmatrix} T_V \\ T_H \end{bmatrix} = \begin{bmatrix} V_\ell^2 & V_c^2 \\ H_c^2 & H_\ell^2 \end{bmatrix}^{-1} \begin{bmatrix} T_{vm} \\ T_{hm} \end{bmatrix} \qquad (20)$$

where matrix notation has been adopted to simplify the results.

At this point it should be emphasized that the corrections for polarization rotation apply only to the antenna beam centers. In addition, for angles of incidence greater than about 10°, the effects of polarization rotation are small for the normally anticipated roll angles. Figure 2 shows a plot of the like polarization factors, expressed as percent polarization, for various incident angles.

Based on the results of this analysis it does not appear that polarization correction processing is warranted for the MFMR radiometer.

Summarizing the results of the MFMR system error analysis, it appears that the significant errors that are present in the unprocessed data are adequately corrected by the present data processing algorithms. Additional sources of error have been identified and appropriate correction techniques have been presented. However, the results of the analysis would indicate that error correction algorithms beyond those currently employed are not necessary in order to provide a useful and meaningful data product.

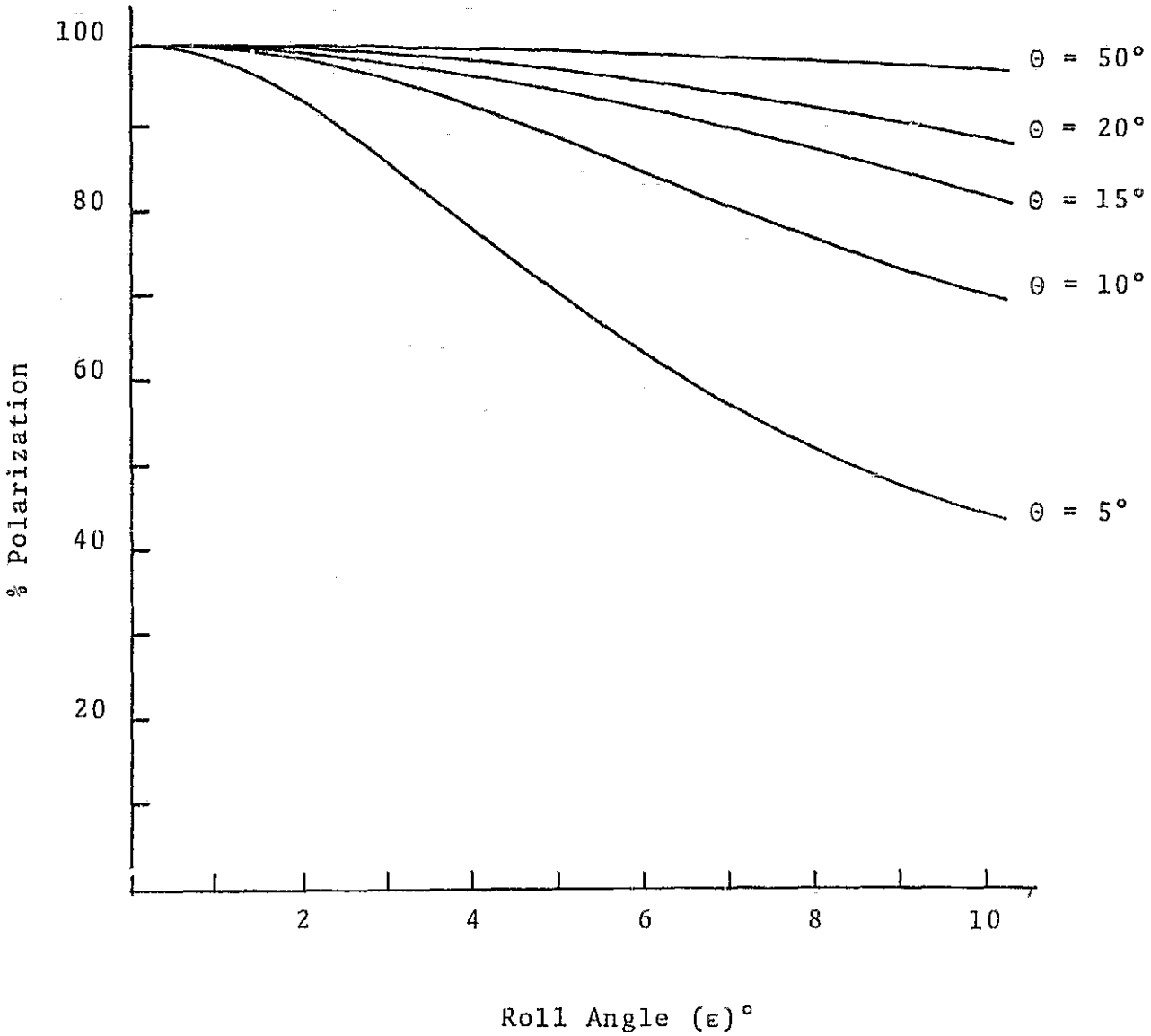

Figure 2. % Polarization vs Roll Angle (At Beam Center) for Various Angles of Incidence

SIGNAL PROCESSING PLAN

The processing requirements for reducing the MFMR output signals to corrected apparent brightness temperatures are such that real-time signal processing is feasible. The PCM data format generated by the system's Multiplexer Encoder and Control Combining Units provide the data in a form directly suitable for digital processing by techniques similar to those developed for the NASA 13.3 GHz scatterometer real-time processor.

The processing algorithms are less complex for the MFMR than for the 13.3 GHz scatterometer in that the dynamic aircraft parameter effects do not affect data calibration. The data available to the processor is in a digital format and does not require additional analog processing. However, the MFMR produces seven independent data channels plus numerous housekeeping and status parameters as opposed to the single pair of orthogonal analog data channels for the radar.

In order to accomplish simultaneous real-time processing of the seven channels of MFMR data, a special purpose digital processor is recommended which will interface with the present MFMR system at the output of the Control Combining Unit (CCU). Data at this point is presently recorded on a single channel of a 14 track magnetic tape recorder. Interfacing with the MFMR here allows for

the CCU output to continue to be recorded as is presently done and provides the option of processing data either directly from the MFMR system or from magnetic tape. The recommended processor implements a computational algorithm which essentially duplicates the present MFMR processing functions with some added features which allow for operator interaction with the processor.

With the exception of mission time, it appears that aircraft parameter data from the ADAS or NERDAS systems will not be required for real-time MFMR data processing. A computer interface for aircraft data is therefore considered as an optional feature for the proposed processor, providing mission time can be derived from another source. One possibility to be suggested is that mission time be included in the CCU PCM format. If accurate tracking of the MFMR footprint or if first-order polarization rotation correction is desired or if mission time is not otherwise available, then an ADAS/NERDAS interface might be included which would increase the complexity of the processor.

In addition to the CCU data channel and possibly an aircraft computer data channel, the only other data required for real-time processing are the radome, antenna, and waveguide loss factors. These data may be stored as look-up tables in real-only memory which can be accessed at the appropriate point in the calibration algorithm by the processor's CPU.

To initiate real-time MFMR data processing, it is envisioned that the operator will enter investigator selectable parameters (e.g. integration or averaging interval) from the front panel, identify which of the radiometers is being operated (all seven channels will normally be processed simultaneously), observe a ready condition, and press a single switch to initiate execution of the processing algorithm.

If valid calibrate and baseline mode data are not present in the processor's random access memory, as will be the case when the processor is first turned on, the processor will request that the operator initiate a calibration sequence for each of the radiometers. At this point the operator will have the option of performing an actual calibration sequence or allowing the processor to default to previously entered or permanently stored calibrate and baseline data. The default option should be of particular value in processing recorded MFMR data.

Figure 3 is a simplified flowchart description of the proposed processing algorithm. The basic features of the program include a mode during which the CPU tests the front panel interface in order to accept manually entered parameters and to respond to a RUN or SELF TEST command. The self test mode allows the processor to exercise all of the system components and interfaces

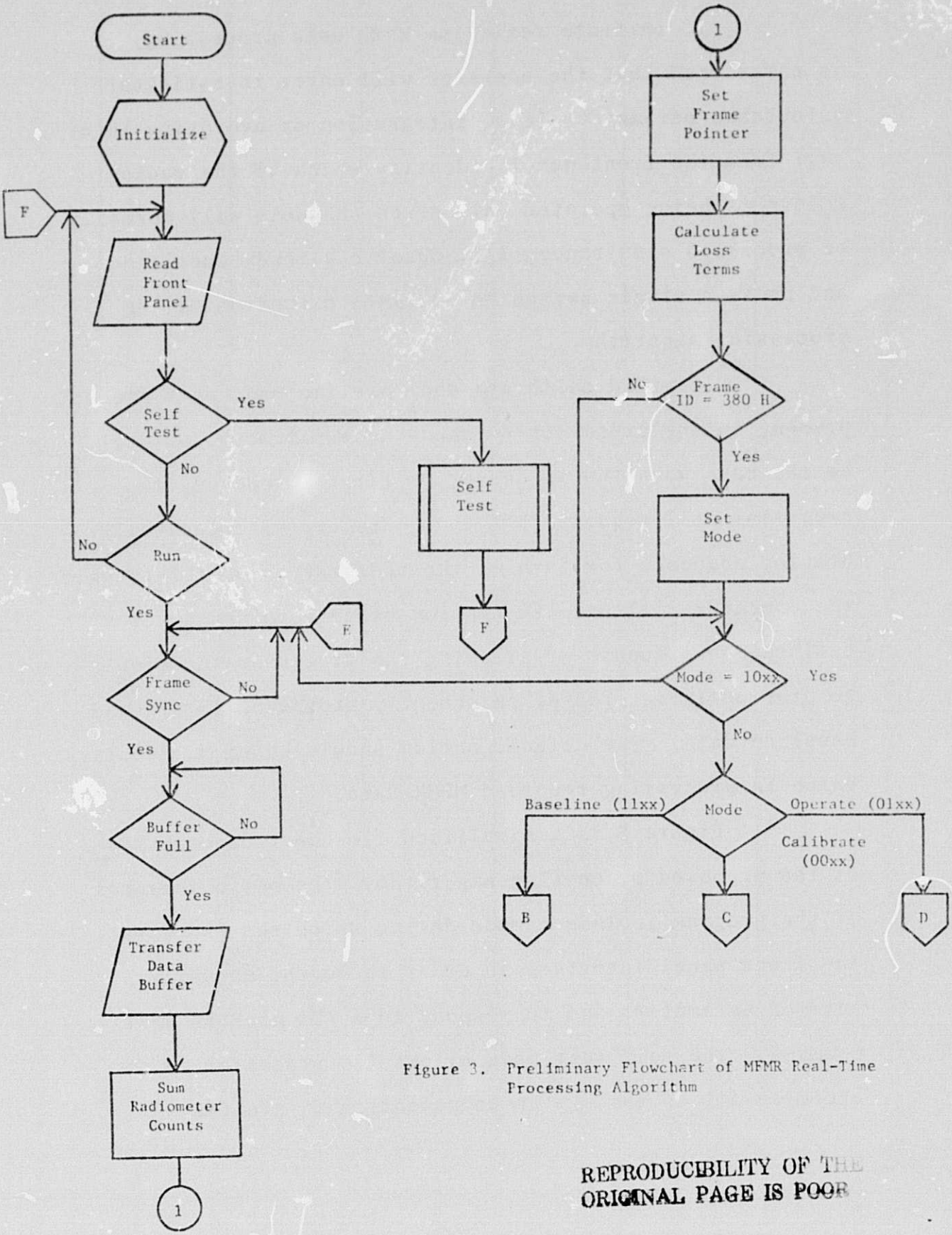

Figure 3. Preliminary Flowchart of MFMR Real-Time Processing Algorithm

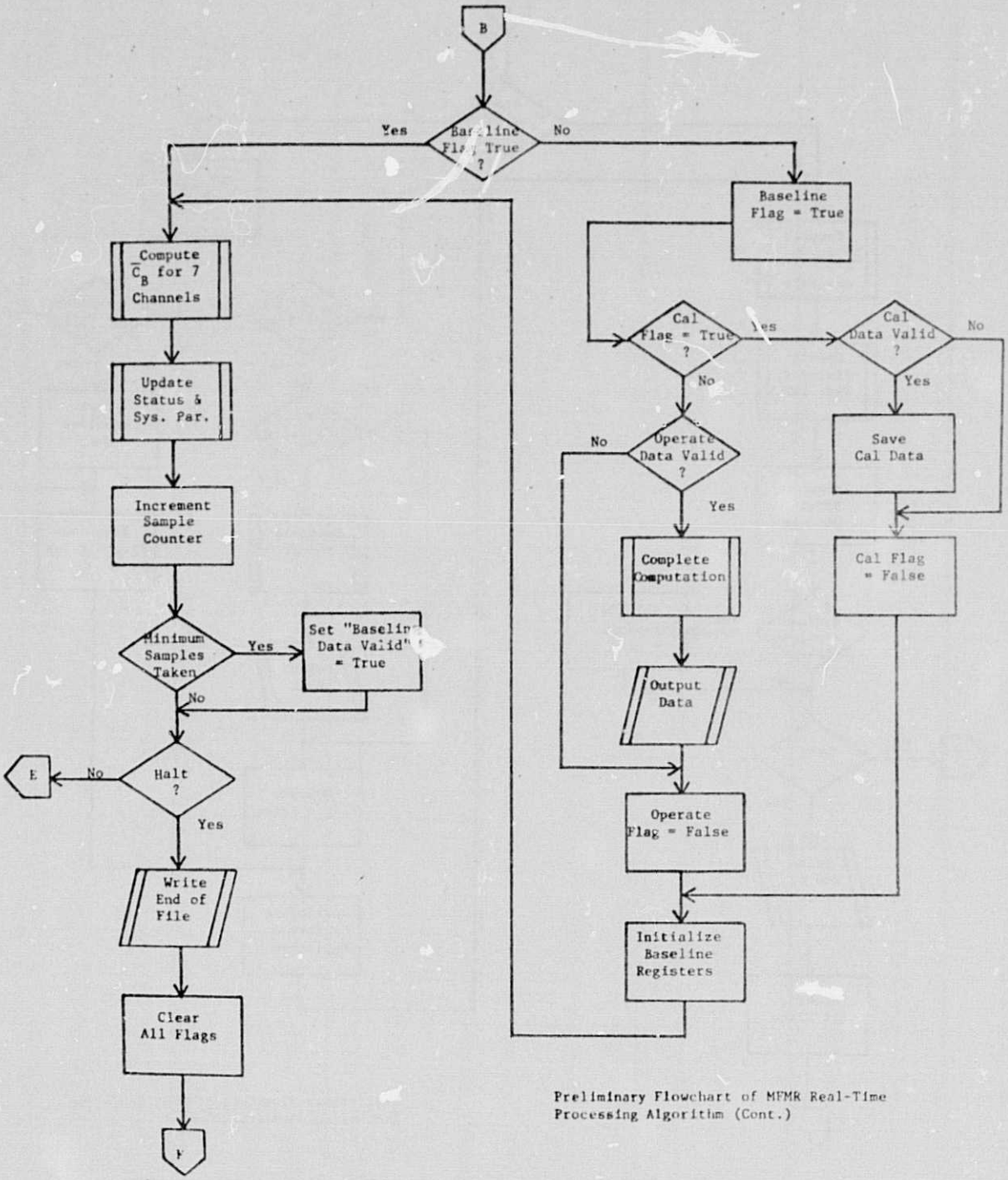

Preliminary Flowchart of MFMR Real-Time Processing Algorithm (Cont.)

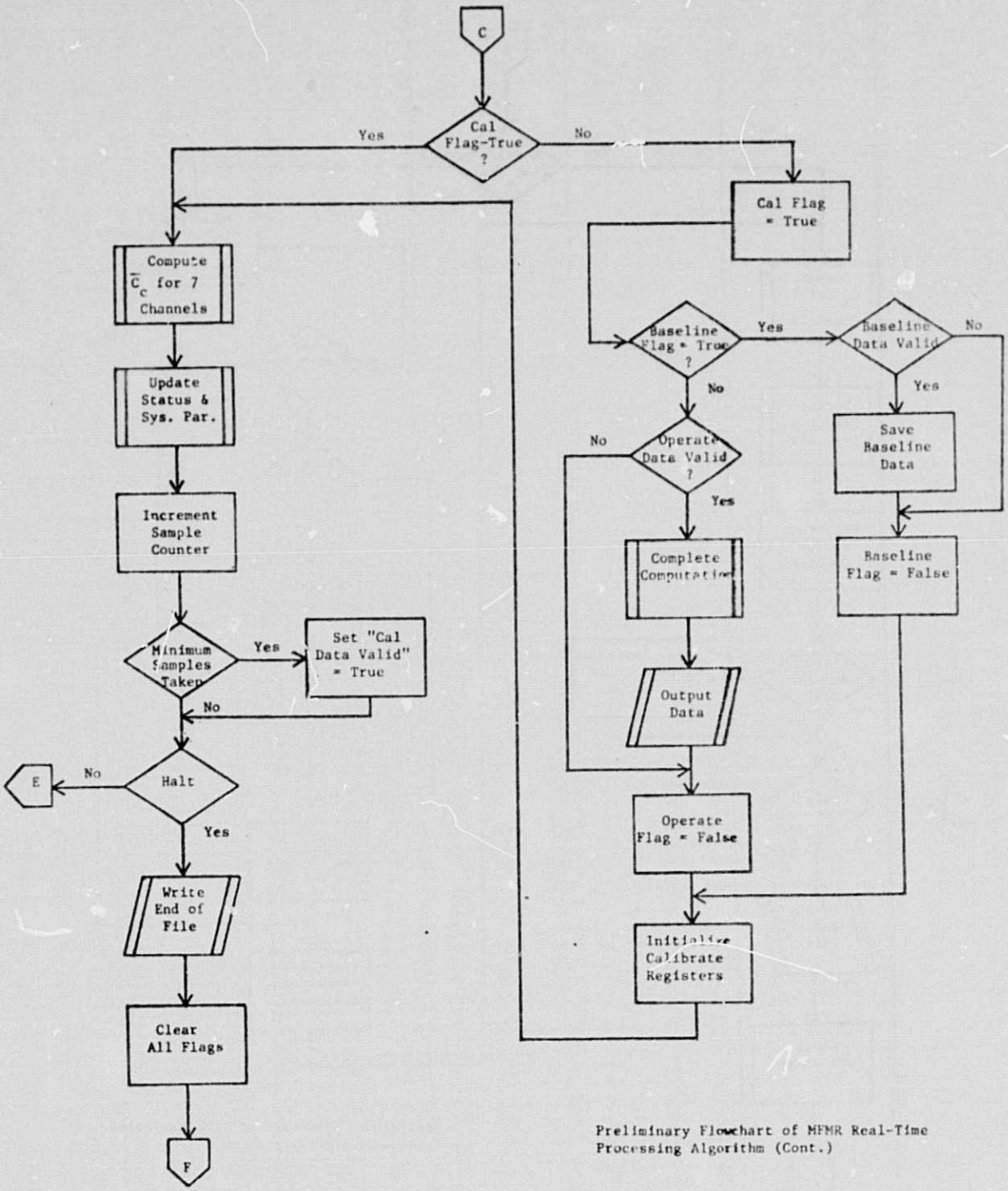

Preliminary Flowchart of MFMR Real-Time Processing Algorithm (Cont.)

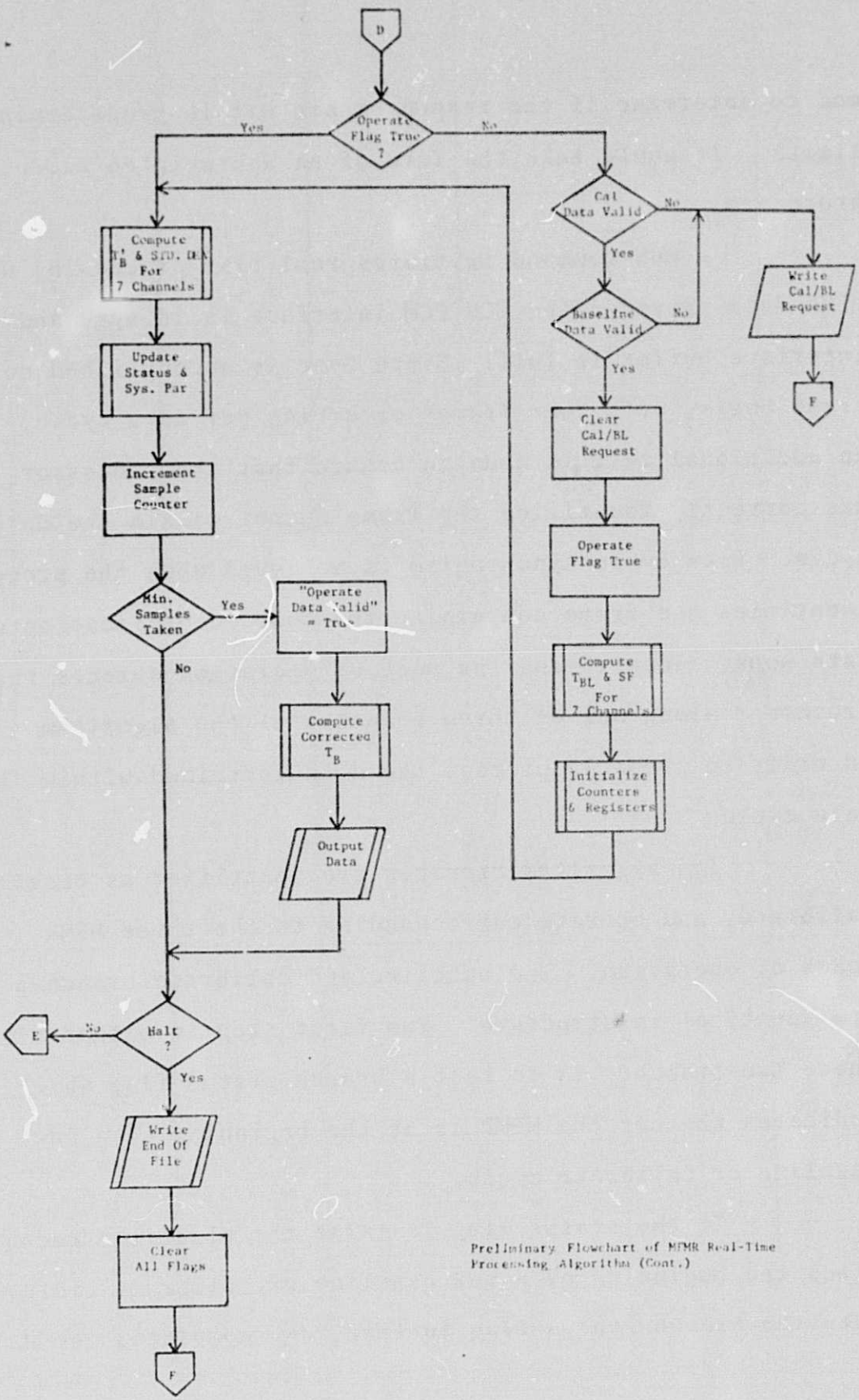

Preliminary Flowchart of MFMR Real-Time Processing Algorithm (Cont.)

and to determine if the responses are within predetermined limits. It would take the form of an abbreviated acceptance procedure.

A RUN command initiates real-time processing of MFMR data provided the CCU PCM interface is in sync and the interface buffer is full. Since Sync is accomplished on a frame basis, with four frames occurring per data cycle, an additional test is made to assure that the processor has correctly identified the frame number within the data cycle. Data cycle synchronism is achieved when the processor identifies the frame containing the mode identification code data word. Identifying the mode of operation directs the processor along one of three branches of the algorithm in order to properly process the data contained within the data cycle.

The algorithm branches are identified as baseline, calibrate, and operate corresponding to the three MFMR modes of operation. The baseline and calibrate branches are identical in structure. The first step in either of these two branches is to test a branch status flag which indicates whether the MFMR is at the beginning of a new baseline or calibrate cycle.

If the status flag is false the algorithm recognizes the beginning of a new baseline or calibrate cycle, sets the branch status flag to true, and completes the data

cycle which has just ended. The branch counters and registers are cleared and the algorithm beings the PCM count (C_B or C_C) averaging process.

At the beginning of the next data cycle, if the mode remains unchanged, the averaging continues until a minimum number of samples have been averaged. Once the minimum sample count has been reached, a "DATA VALID" status flag is set, while the averaging process continues until the MFMR mode is changed.

At the end of each cycle the CPU tests for a HALT command. If the HALT switch has been depressed, the processor terminates the processing sequence, writes appropriate end-of-file messages, clears all status flags, and returns to an idle condition.

In the operate branch of the processing algorithm, a branch status flag is also tested to indicate the beginning of a new operate mode cycle. At the beginning of the cycle the processor checks for valid calibrate and baseline data before proceeding with data reduction. If valid data is not present the processor requests via a front panel indicator that a baseline/calibrate cycle be initiated. The processor returns to the beginning of the algorithm to pick up the next data frame and continues to test appropriate flags until valid baseline and calibrate data is received or until a default option is selected by the operator.

With valid baseline and calibrate data present, the operate branch of the algorithm begins by computing T_{BL} and SF as in equation (2). The sample counter and registers are cleared and data averaging proceeds. The averaging technique recommended for implementation is that of a "moving window" which forms a new average by adding the most recent data sample, subtracting the Nth oldest sample, and dividing the sum by N, where N is the number of samples within the τ second time window. This average may be expressed analytically as

$$\overline{T_B'}(n) = \frac{1}{N} \sum_{i=n}^{N+n-1} T_B'(i) \qquad (21)$$

The standard deviation for the N samples in (21) is expressed as

$$\sigma_{T_B'}(n) = \sqrt{\frac{\sum_{i=n}^{N+n-1} T_B'^2(i) - N\,\overline{T_B'}^2(n)}{N-1}} \qquad (22)$$

After the first N samples are received, the processor computes corrected apparent temperatures for each data channel according to equation (4). These data values are then identified by time, angle, frequency, and polarization and are formatted for output to a magnetic tape recorder and, selectively, to an analog strip chart.

Again, the processing algorithm may be terminated by a HALT command, returning the processor to its initial idle or hold state.

The primary output data product will consist of magnetic tape recorded values of corrected average apparent temperature for each radiometer channel. The data will be identified by the time corresponding to last sample of each averaged temperature along with the angle of incidence, frequency, polarization, and standard deviation of the averaged samples. In addition, the relevant parameters (i.e. waveguide temperatures, etc.) used in the correction calculation will be included in the output data frame for each temperature value.

The only additional processing requirement for providing the investigator with reduced MFMR data will be to read the magnetic tape, format the data in a convenient manner, and print a hard copy of the recorded data.

SYSTEM DESIGN

The preliminary design concept for the MFMR real-time processor is based upon the development of special purpose digital computers built around a flexible micro-processor chips. In Figure 4 a block diagram is presented which depicts the MFMR system as it would interface with the real-time processor. As previously noted the real-time processor interfaces with the present MFMR system at the CCU output. An optional aircraft interface is also shown should such be necessary.

The PCM interface and buffer, as shown in Figure 4 performs two important functions. First, the interface synchronizes with the PCM data stream and clocks the data into one of two buffer registers. Secondly, by means of this double buffering action, the interface allows the CPU to decommutate the PCM data in a short period of time relative to the data frame length. This allows real-time processing to be accomplished during the time in which a second frame of data is being stored in the second buffer.

The remaining structure of the processor is straightforward. It consists of a CPU (comprised of an microprocessor chip and associated control logic), an estimated 6K bytes of read-only memory, 2K bytes of random access memory, an operator's control panel and interface, and an output interface to the recorders and display.

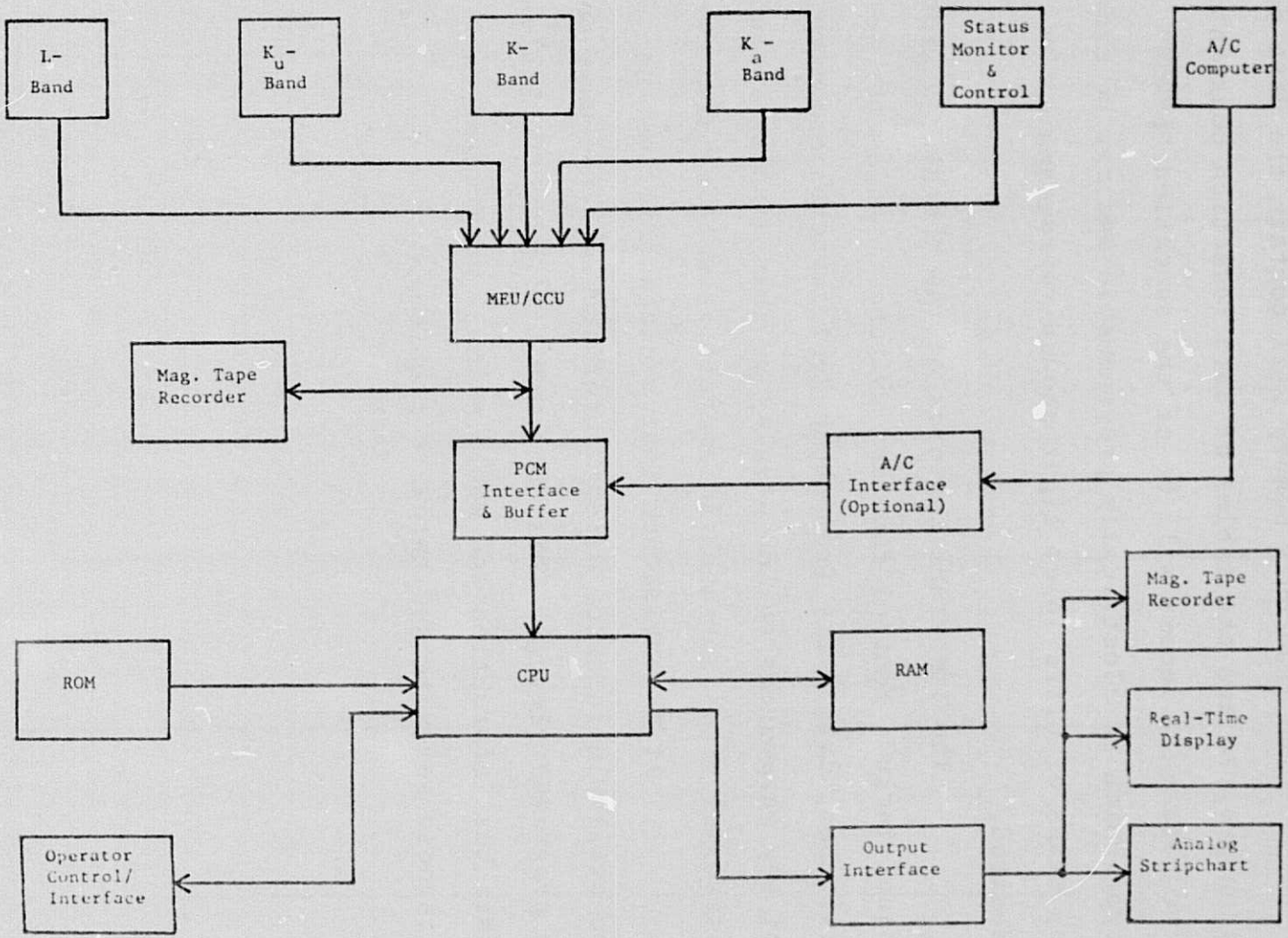

Figure 4. Block Diagram of MFMR System with Proposed Real-Time Data Processor

The read only memory will contain the data reduction program and the tables of data reduction constants. The read only memory will be of the so-called "EPROM" type which is electrically programmable and may be erased by means of ultraviolet light should reprogramming be desired.

The important features of the operator's front panel include control function switches, radiometer selection switches, data entry from thumbwheel switches and display of key parameters on LED displays. This display includes status of processor and radiometers as well as data output.

It is envisioned that a diagnostic test set would be available to allow direct interface with the unit on a programmer level. This unit would display CPU status, data bus information and would allow a programmer to diagnose software and hardware problems.

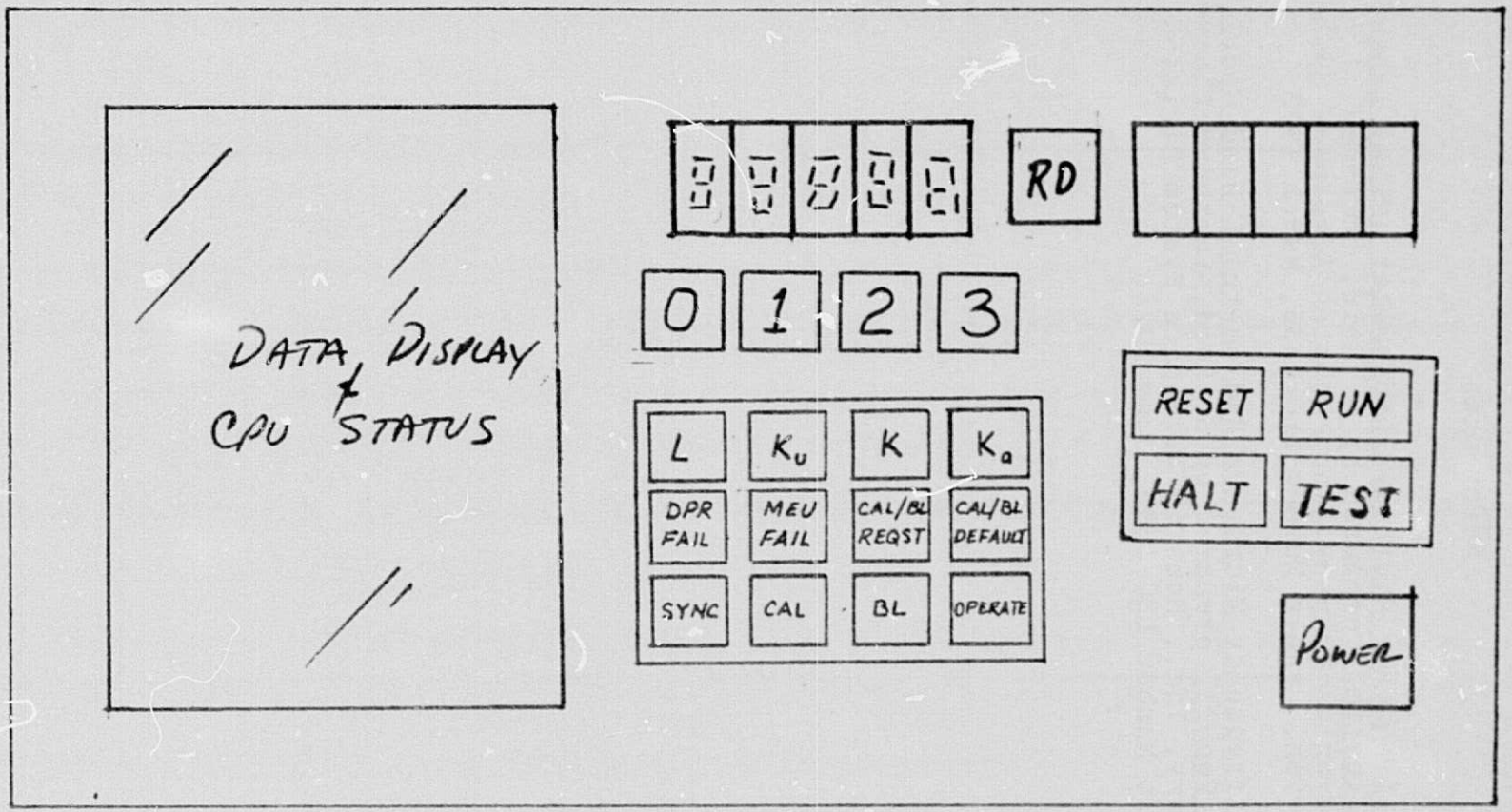

Figure 5. A possible front panel configuration for the recommended MFMR data processor.

References

1. Multifrequency Microwave Radiometer (MFMR) L-band Modification, prepared by S. Reid, Lockheed Electronics Company, Inc., Houston Aerospace System Division, Report Number LEC-0336, March 1973.

2. Multifrequency Microwave Radiometer L-band Modification Test Report, prepared by S. Reid, Lockheed Electronics Company, Inc., Houston Aerospace System Division, Report Number LEC-3353, June 1974.